Effect of Laser-Induced Crystallinity Modification on Biodegradation Profile of Poly(L-Lactic Acid)

Shan-Ting Hsu

Huade Tan

Y. Lawrence Yao

Department of Mechanical Engineering,
Columbia University,
New York, NY 10027

Poly(L-lactic acid) (PLLA) is of interest in drug delivery applications for its biodegradable and biocompatible properties. Polymer-controlled drug delivery relies on the release of embedded drug molecules from the polymer matrix during its degradation. PLLA degradation exhibits an induction period, during which an insignificant amount of degraded products and embedded drug can be released. Due to this induction period, drug release is initially nonlinear, a complication in drug delivery applications. PLLA degradation is a function of crystallinity, such that control over its crystallinity tailors drug release over time. In this study, the effect of laser-induced PLLA crystallinity reduction on degradation is investigated. Samples having lower surface crystallinity are shown to have higher rates of molecular weight reduction and earlier mass loss than nonlaser-treated samples, as observed from gel permeation chromatography and mass change. Wide-angle X-ray diffraction measurements show that crystallinity increases with degradation. A numerical model is implemented from hydrolysis and diffusion mechanisms to investigate the effect of laser irradiation on biodegradation. Controlled laser treatment of PLLA offers a method for constant drug release through the reduction of surface crystallinity. [DOI: 10.1115/1.4025394]

Keywords: poly(L-lactic acid), laser treatment, biodegradation, crystallinity, drug delivery

1 Introduction

PLLA is attractive in drug delivery, food packaging, and tissue engineering applications because of its biocompatible and biodegradable properties. PLLA is especially of interest in drug delivery applications because it hydrolyzes in the human body into lactic acid, a product that is excreted by the body with no toxicity. In drug delivery applications, drugs are embedded in a polymer matrix and released as it degrades. Biodegradable polymers offer a means to control the drug delivery in time [1]. Drug release from biodegradable polymer exhibits an induction period, a duration of time required for water molecules to penetrate into the matrix before degradation can occur [2]. During this time, embedded drugs are not released at a linear rate.

PLLA degradation in a physiological environment occurs via hydrolysis, in which water penetrates into the polymer matrix, attacking the ester bonds and causing chain scission. Water molecules readily penetrate into the amorphous region but hardly into the crystalline region, because the polymer chains are highly packed and densely ordered in crystals [3]. Degradation of ester bonds occurs faster in the amorphous phase because of its more permeable structure [3]. Hydrolysis in the crystalline phase begins at the fold surfaces and progresses inward as controlled by chain scission [4]. Hydrolysis in the crystalline phase occurs less preferentially than in the amorphous phase. A sample composed of both crystalline and amorphous phases will more rapidly undergo hydrolysis in the amorphous phase than the crystalline phase [4].

PLLA hydrolysis is accelerated by autocatalysis [5]. The rate of hydrolysis increases as the concentration of reaction products increases. Hydrolysis of polyester produces shorter chains with acid and alcohol end groups. Acid end groups dissociate, leading to an acidic environment, which accelerates hydrolysis. Therefore, the diffusion of shorter chains out of the polymer plays a key role in controlling the overall degradation rate. Another factor that complicates biodegradation is the increase of crystallinity during degradation [6,7]. Preferential degradation in the amorphous region leaves the crystalline phase behind, leading to a mostly crystalline material [4]. Chain scission as a result of degradation also increases chain mobility, which facilitates crystallization in the amorphous phase.

Because changing the surface crystallinity of PLLA has the potential to tailor the initial degradation rate, laser heat treatment to reduce surface crystallinity is of interest. PLLA crystallinity reduction by laser irradiation with infrared (IR) and green wavelengths has been quantified through wide-angle X-ray diffraction (WAXD) measurements [8]. The same effects have been observed by excimer laser processes operating at ultraviolet (UV) wavelengths with photon energies higher than bond energies [9,10]. It has been shown that surface crystallinity can be reduced with no measurable chemical modifications due to the low radical mobility in the crystal structure [10]. The effects of laser treatment on polymer degradation over time have yet to be studied.

The objective of this work was to investigate the effects of laser surface treatment on PLLA degradation, characterized by the change in mass, molecular weight (MW), and crystallinity. Since PLLA degradation behaves similarly at elevated temperatures [11], degradation was conducted at an elevated temperature to shorten the total test time. MW and crystallinity were determined through gel permeation chromatography (GPC) and WAXD, respectively. A numerical model was developed to capture the degradation process.

2 Background

2.1 Laser Melting of Polymer. Polymer melting is an amorphization process in which crystalline polymer chains detach from crystals. Crystalline polymer chains are held by weak van der Waals forces and hydrogen bonds, which are broken during
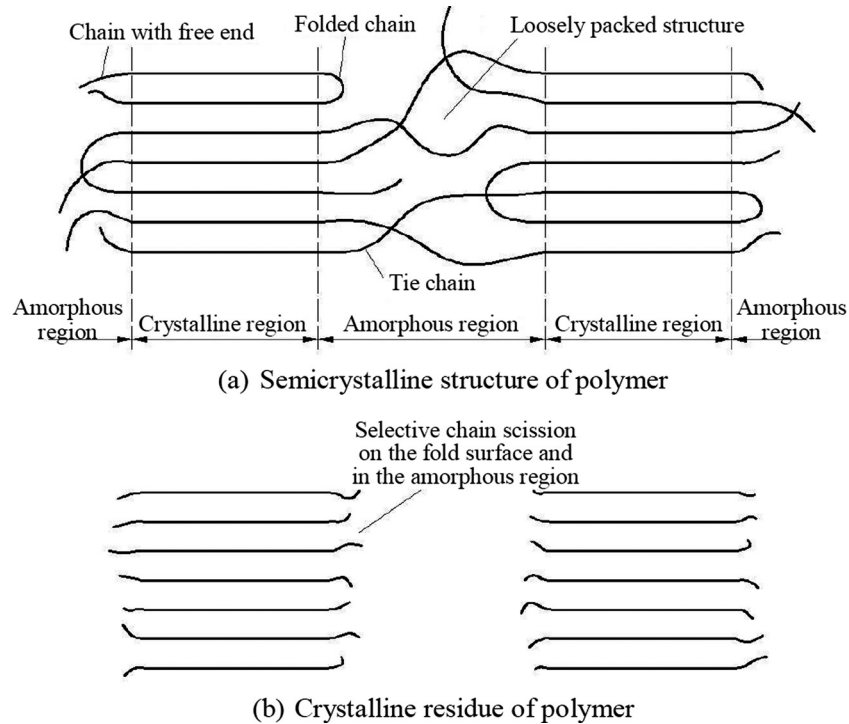
Fig. 1 Schematic representation of (*a*) semicrystalline structure and (*b*) crystalline residue of polymer after hydrolysis, which preferentially occurs in amorphous region and on crystal fold surface, leading to mass loss [19]

melting to form an amorphous structure. Melting initiates at the crystal fold surface, followed by the progressive unfolding of chains toward the center of the crystal. Polymer melting occurs within nanoseconds [12], and thus nanosecond laser treatment is used to induce polymer melting. Crystallinity is reduced after laser melting as a result of slow crystallization kinetics compared with the rapid melting and cooling during laser processing [7–10].

Polymer absorption of photons with energies exceeding the bond energy risk breaking chemical bonds. In PLLA, this reaction occurs between two CH_3CHCOO units. If no oxidation occurs during processing, the separated CH_3CHCOO units may recombine. According to the cage effect, high PLLA crystallinity has been shown to reduce the amount of bond breaking and lead to nonmeasurable chemical modifications under UV laser treatment [10].

2.2 Biodegradation of Polyester. PLLA is a biodegradable polyester, which breaks down in the human body through hydrolysis. Water molecules attack the ester bonds via the following reaction

$$
\begin{array}{c}
\text{—C—C—O—C—C—O—} + H_2O \longrightarrow \text{—C—C—OH} + HO\text{—C—C—O—}
\end{array}
\tag{1}
$$
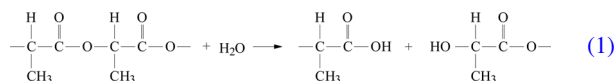
Hydrolysis causes chain scission and produces shorter chains with carboxylic (-COOH) groups and alcohol (-OH). The rate of hydrolysis is proportional to the number of ester bonds present in each monomer constituting the polymer. The number of reactive bonds in the polymer decreases as hydrolysis goes on. Hydrolysis depends on the molar concentrations of the monomer still present in the polymer chain, C_e, and water, C_w [13], at the rate of

$$
\frac{dC_e}{dt} = -k_1 C_e C_w
\tag{2}
$$

where the constant k_1 depends on temperature and does not vary with reaction. Carboxylic end groups generated from this reaction

have a high degree of dissociation and can act as a catalyst to accelerate the hydrolysis. Hydrolysis of polyesters may become autocatalytic if carboxylic end groups remain in the bulk [14]. During autocatalyzed hydrolysis, the reaction rate depends on the concentration of the carboxylic end groups, C_{COOH}, as well. The rate of autocatalyzed hydrolysis is given by [15]

$$
\frac{dC_e}{dt} = -k_2 C_e C_w (C_{COOH})^n
\tag{3}
$$

where k_2 is the rate constant for the autocatalysis reaction, and n accounts for the dissociation of the carboxylic groups and can be used as an empirical parameter to reflect the reactions [16].

Amorphous chains hydrolyze in three stages before generating monomers [17]. In stage 1, chain scission commences in the intact amorphous chains, resulting in the breaking of amorphous tie chains. In stage 2, chain scission occurs on already broken amorphous chains, creating unattached oligomers. In stage 3, hydrolytic reactions occur on short amorphous segments protruding from the crystals and the oligomers produced in stage 2. Hydrolysis in this stage generates highly mobile monomers, which can diffuse out of the polymer matrix.

PLLA can be semicrystalline, and the amorphous region experiences a higher hydrolysis rate than the crystalline region [3,18]. Hydrolysis of the amorphous phase occurs randomly but occurs preferentially in the crystal phase at the fold surfaces. A schematic representation of semicrystalline polymer chains before and after extensive hydrolytic degradation is given in Fig. 1 [19]. Random hydrolysis generates chains with a wide length distribution; preferential hydrolysis on fold surfaces can lead to the chains representing the integral folds the crystalline residues [18,20]. Mobile segments reorganize themselves from a disordered to an ordered state due to intermolecular hydrogen bonds and van der Waals forces, leading to crystallization during hydrolysis [3].

3 Numerical Model

A 2D symmetric model is developed to investigate the effect of laser treatments on biodegradation profiles. Laser energy absorbed

by semitransparent bulk PLLA generates heat governed by the heat equation

$$\rho C_p(T)\frac{\partial T}{\partial t} = \nabla \cdot (k\nabla T) + q(z,t) \qquad (4)$$

where ρ is mass density, $C_p(T)$ is specific heat as a function of temperature T, k is thermal conductivity, $q(z,t)$ is the laser power density as a function of depth from the laser irradiated surface z and time t, expressed as

$$q(z,t) = Q_0 e^{-\alpha z + \beta\left(\frac{t}{t_p}-2\right)^2} \qquad (5)$$

where Q_0 is peak power density, α is absorption coefficient, t_p is pulse width, and β is $-4ln2$. Parameters used in Eqs. (4) and (5) and the change in $C_p(T)$ during the phase transition are further detailed in Ref. [10]. Polymer crystals melt within a temperature range, from T_m to $T_m + \Delta T_m$. The crystal fraction melting in a temperature increment dT_m within T_m and $T_m + \Delta T_m$ can be expressed as $\phi(t, T_m)dT_m$. The total crystallinity is then $\Phi(t) = \int_{T_m}^{T_m+\Delta T_m} \phi(t, T_m)dT_m$. The change in $\phi(t, T_m)$ during melting is given by [21]

$$\frac{d\phi}{dt}(t, T_m) = -R_m(\Delta T)\phi(t, T_m) \qquad (6)$$

The melting rate coefficient R_m is a function of superheating, $\Delta T = T - T_m$, expressed as $R_m = R_m(\Delta T)$ if $\Delta T > 0$ and $R_m = 0$ if $\Delta T < 0$. Molecular dynamics simulations have suggested that crystallinity decreases within nanoseconds, and R_m is of the order of 10^9s^{-1} [12]. Spatially resolved crystallinity after laser processing is imported into the degradation model as the initial condition.

Biodegradation is captured using a phenomenological model [16]. Semicrystalline PLLA is modeled to be consistent of seven species during degradation: nondegraded amorphous chains, degraded amorphous chains in stages 1, 2, and 3 [17], crystalline chains, monomers, and water molecules. Nondegraded and degraded amorphous chains hydrolyze via the scission of the ester bonds contained in the species but have zero diffuse-ability due to restricted mobility. Monomers have high mobility. Amorphous polymer chains crystallize during degradation. Crystalline polymer chains cannot diffuse and are assumed to hydrolyze ten times slower than amorphous chains [22], generating chain scission on the crystal fold surface. Water molecules are assumed abundant in time and space, and the size distribution of polymer chains is neglected. Acid end groups of the monomers, generated during chain scission, accelerate the hydrolysis through autocatalysis. Assuming water concentration is constant temporally and spatially, the molar concentration of the nondegraded amorphous chain is expressed as

$$\frac{dC_0}{dt} = -\gamma_0 C_0 - \varepsilon_0 C_0 C_m^n - \kappa_0 \frac{dC_c}{dt} \qquad (7)$$

where C_0 and C_c are the molar concentrations of monomers in the nondegraded amorphous chains and crystalline chains, respectively. The dissociation of the acid end groups n is assumed to be unity. The first, second, and third terms on the right of Eq. (7) account for rates of nonautocatalysis, autocatalysis, and crystallization from amorphous chains, respectively. Values of γ_0, ε_0, and κ_0 are the corresponding phenomenological rate constants. Hydrolysis of nondegraded amorphous chains, Eq. (7), generates degraded amorphous chains in stage 1, which is then hydrolyzed into stage 2 and contributes to crystallinity. Similarly, hydrolysis of chains in stage 1 leads to stage 2, and hydrolysis of chains in stage 1 leads to stage 2. Part of the hydrolyzed chains also crystallizes during hydrolysis. The molar concentration of monomers in each stage is expressed as

$$\frac{dC_i}{dt} = (\gamma_{i-1} + \varepsilon_{i-1}C_m^n)C_{i-1} - (\gamma_i + \varepsilon_i C_m^n)C_i - \kappa_i \frac{dC_c}{dt} \qquad (8)$$

where $i = 1, 2,$ and 3, representing degradation stages 1, 2, and 3, respectively. C_i is the molar concentration of the monomers in stage i. γ_i, ε_i, and κ_i are the phenomenological rate constants accounting for nonautocatalysis, autocatalysis, and crystallization due to hydrolysis in stage i, respectively. During degradation, the crystallization of linear polyesters is modeled using the Avrami equation [6], $\phi = 1 - \exp(-k_c t^m)$ where ϕ is monomer fraction in the crystalline domain, k_c is the Avrami constant, and m is the Avrami exponent [23]. Hydrolysis of the stage 3 species generates monomers, which do not connect to other monomers and have high mobility to diffuse out of the polymer matrix. Assuming Fick's second law for monomer diffusion, which predicts the change of monomer concentration with space and time, the molar concentration C_m of the monomers with high mobility is modeled by

$$\frac{dC_m}{dt} = (\gamma_3 + \varepsilon_3 C_m^n)C_3 + \nabla \cdot (D\nabla C_m) \qquad (9)$$

where D is the monomer diffusivity. Appropriate units are used for the phenomenological rate constants so that each term in Eqs. (7)–(9) is in mole per volume per time. The values of the rate constants are selected to capture experimental results [16].

The coupled partial differential Eqs. (4) and (6) are solved to determine crystallinity change due to laser treatments. Solutions of these equations are used as initial conditions to solve the coupled Eqs. (7)–(9) to capture degradation profiles. The two sets of coupled equations are solved through the finite element method in COMSOL Multiphysics 4.1. A 2D axial symmetric domain is used, in which the 1-mm × 5-mm film is immersed in a 10-mm × 10-mm aqueous medium. Laser treated area covers both sides of the film. The film is initially composed of nondegraded crystalline and amorphous chains with crystallinity determined experimentally. Monomers generated during degradation can diffuse out of the film into the surrounding aqueous medium. The time domain in the simulation is 14 days.

4 Materials and Methods

PLLA granules (medical grade with a viscosity of 1.8 dl/g) were provided by PURAC and used as received. PLLA samples were prepared through thermal compression of PLLA granules under 5.7×10^4 Pa at $180\,^\circ\text{C}$ for 4 h and cooled down in air. The cooling process lasted for around 2 h to reach room temperature. Crystals developed during the cooling process. The obtained sample was around 80 mg and 1 mm thick. Laser treatment was conducted by a KrF excimer laser with 248 nm wavelength and 25 ns pulse width. Laser spot size is 1 mm × 1 mm. Both sides of the sample were scanned by laser irradiation. The homogenized excimer laser beam had a spatially uniform intensity favorable for a uniform surface treatment. The sample was radiated by a single pulse in argon atmosphere with a flow rate of 0.4 standard cubic meters per hour to prevent oxidation. To determine crystallinity, WAXD measurements were made using an Inel X-ray diffractometer to determine crystallinity. Monochromatic CuKα radiation with wavelength $\lambda = 0.15418$ nm at 40 kV and 30 mA was used. The chemical compositions of the PLLA samples were measured using X-ray photoelectron spectroscopy (XPS, PHI 5500 ESCA). From XPS measurements, the O_{1s} and C_{1s} spectra were captured, and the takeoff angle was 45 deg.

During degradation tests, each sample treated with 3-J/cm^2 laser energy was placed in a vial and fully immersed in a 10-mL phosphate-buffered saline (PBS) with a pH of 7.4 purchased from Life Technologies. Vials were placed in a water bath at $70\,^\circ\text{C}$, and the PBS was changed every 2 days. The degradation periods are 0.5, 1, 1.5, 2, 3, 5, 8, 11, and 14 days. After degradation, samples were dried in vacuum at room temperature for 2 days. The sample
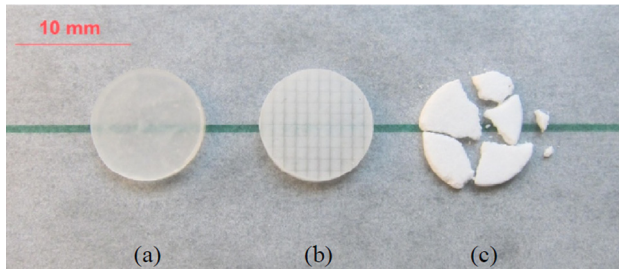
Fig. 2 Nondegraded PLLA sample (*a*) before and (*b*) after laser treatment with a fluence of 3 J/cm². Laser-irradiated spots show less transparency due to increased surface roughness. The laser-treated sample degraded for 14 days is given in (*c*) and its high crystallinity reduces the transparency.

Fig. 3 PLLA crystallinity and the ratio of O_{1s} to C_{1s} as a function of laser fluence. The error bar represents the standard deviation of 3 data points.

mass was recorded before and after vacuum drying. The weight-average MW (M_w) and number-average MW (M_n) were determined in tetrahydrofuran (THF) from GPC at room temperature. Crystalline PLLA was first dissolved in methylene chloride and rapidly dried with a rotary evaporator to obtain the amorphous form with higher solubility in THF. PLLA/THF solutions were prepared with 1 mg/1 ml concentration for GPC measurements. Crystallinity is determined by the WAXD, and morphology is observed using stereomicroscopy and optical profilometry.

5 Results and Discussion

5.1 Effect of Laser Irradiation on Crystallinity and Chemical Modifications. Images of samples prepared by thermal molding before and after laser treatment as well as after 14 days of degradation are presented in Fig. 2. After thermal molding, the M_n and M_w are slightly reduced from 133 kg/mol to 129 kg/mol and from 142 kg/mol to 137 kg/mol, respectively. Both laser-treated and nonlaser-treated samples were prepared through the same process, and therefore the effect of thermal molding is not considered to influence subsequent experimental results. The nonlaser-treated sample is translucent because of the existence of crystalline phase. Laser treatment generates opaque spots, a result of strong light scattering from the roughened surface as confirmed by optical profilometry. Roughness is induced by laser surface melting and resolidification. To determine laser penetration depth, spectrophotometry has been conducted. At 248 nm (laser wavelength), the absorption coefficient is $10 \, \text{mm}^{-1}$, which corresponds to a penetration depth of around $100 \, \mu\text{m}$. To study the effect of laser treatment on crystallinity modification, WAXD has been conducted on the nonlaser-treated and laser-treated samples before degradation. Crystallinity is calculated based the WAXD results [24], as given in Fig. 3. It should be noticed that X-ray penetration depth of PLLA is calculated to be around 1 mm based on the linear absorption coefficients and mass densities of the atoms composing PLLA [24]. The grazing angle of incident X-ray is adjusted to be as small as possible to emphasize the effect of the laser melted layer.

To investigate possible chemical modifications under laser irradiation, XPS measurements are performed. Chemical reactions caused by laser irradiation with photon energies higher than the bonding energies lead to the reduction of the ratio of O_{1s} to C_{1s}, as shown in Fig. 3. Based on the permutation test at 90% significance level, fluence between 2.6 and 3.0 J/cm² causes significant crystallinity decrease and insignificant O/C change as compared with the nonlaser-treated sample. The drop of O/C is indicative of chemical modifications due to laser treatment. The chemical modifications of PLLA samples remain insignificant below 3.0 J/cm² due to the cage effect, which states that free radicals generated by the dissociation of molecules cannot move apart because of the confinement of surrounding molecules [10]. This results in the recombination of the dissociation products, which then return to the
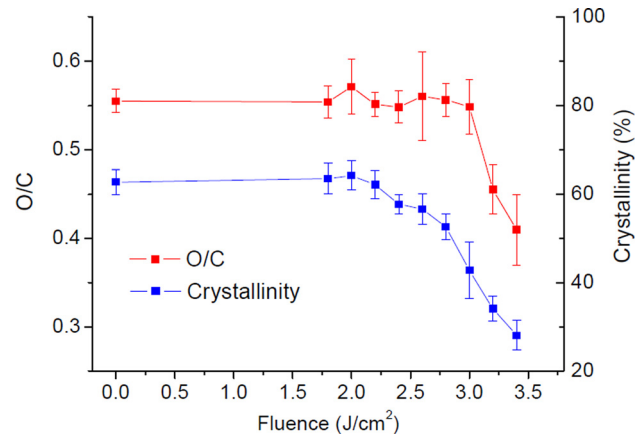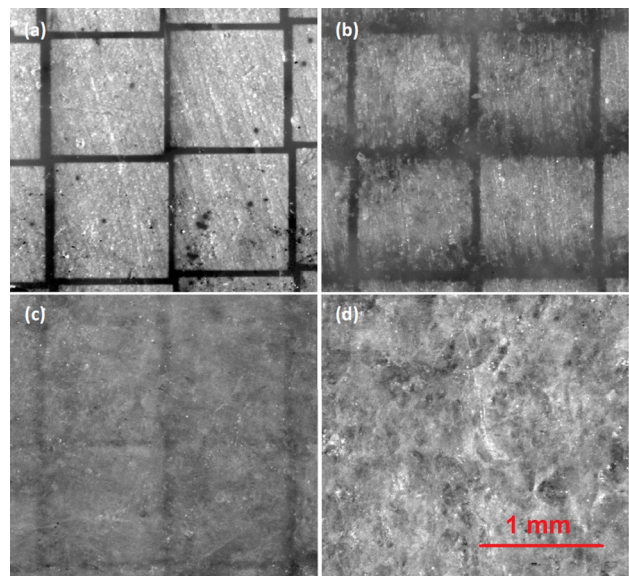

Fig. 4 Surface morphology of the laser-treated sample (*a*) before and after degradation for (*b*) 3, (*c*) 8, and (*d*) 14 days under the stereomicroscope. The squares in (*a*) are laser spots. The edges of laser spots become less defined with degradation period, suggesting the erosion of laser melted layer. Degradation in the nonmelted bulk volume occurs in the later stage.

initial state. A fluence of 3.0 J/cm² induces the maximum amorphization with nonmeasurable chemical modifications and is used as the energy level to treat samples in this study.

5.2 Effect of Laser Irradiation on Degradation.

5.2.1 Modification of Morphology. Laser-treated samples after degraded for 14 days are shown in Fig. 2. A uniformly opaque morphology is observed as a result of higher crystallinity developed during degradation. By the end of the degradation test, the appearance of laser-treated sample is similar to nonlaser-treated sample, and laser spots are invisible, as given in Fig. 2(*c*). Detailed morphology investigations are given by stereomicroscopic images of laser-treated samples as a function of degradation period in Fig. 4. A laser-treated sample before degradation is given in Fig. 4(*a*). The 1-mm × 1-mm square spot is generated by laser irradiation. The grid pattern is the spacing between laser spots and is not laser treated. As degradation progresses, spot edges become less defined, Fig. 4(*b*), suggesting the degradation
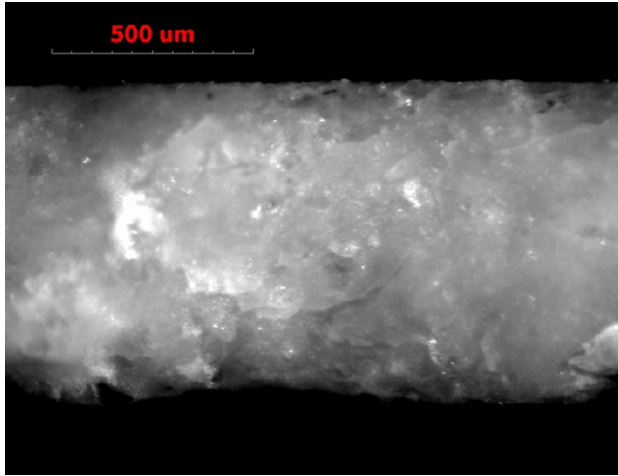
Fig. 5 Cross section of the laser-treated sample degraded for 14 days. The bulk remains solid, suggesting that autocatalysis is not dominant.

and erosion (mass loss) of laser-melted layer. After 8 days, Fig. 4(c), spot edges become more indistinct than samples degraded for shorter periods. During prolonged testing, the laser-melted layer is eroded and degradation starts to occur in the nonmelted volume below. Eventually, the morphology of laser-treated sample, Fig. 4(d), is similar to that of the nonlaser-treated sample. The cross section of a laser-treated sample after being degraded for 14 days is given in Fig. 5. It is observed that the bulk remains solid, which suggests that autocatalytic degradation is not dominant as a result of easy diffusion of acidic monomers out of the sample.

5.2.2 Modification of Crystallinity. To investigate the changes in crystallinity during degradation, WAXD measurements have been conducted on samples after regular degradation intervals, as depicted in Fig. 6. Before degradation, laser treatments cause surface melting and a reduced crystalline peak, as given in the dashed black curves in Figs. 6(a) and 6(b). For both types of samples, crystalline peaks become more prominent with time, suggesting the occurrence of crystallization during degradation. Sample crystallinity, as calculated from WAXD measurements based on Ref. [24], is given as a function of time in Fig. 7, which shows that crystallinity increases with degradation period, in agreement with Fig. 6. The degradation test was conducted at 70 °C, which is higher than PLLA glass transition temperature; therefore, the samples are annealed during degradation, which serves as one factor causing the increased crystallinity. Simply annealing, however, does not explain the nonmonotonous crystallinity increase on day 0.5 and day 3 for laser-treated sample and day 8 for nonlaser-treated sample. For both types of samples, a significant increase of crystallinity is observed at day 0.5, when the sample MW begins to decrease, as is discussed in Sec. 5.2.3. The decrease of MW favors chain reorganization and crystallization and increases crystallinity. Lower crystallinity and greater amounts of crystallizable material in nondegraded samples also favors crystallization [25]. Crystallization slows between day 0.5 and day 5 for the nonlaser-treated sample, because part of the amorphous chains is less crystallizable, including the rigid amorphous phase (RAP) [26] and entangled chains. The RAP and entangled chains hinder chain movements and make it difficult for amorphous chains to relax and crystallize. Crystallinity also significantly increases at day 8 for the nonlaser-treated sample, and day 3 for the laser-treated sample. At this stage, the amorphous chains diffuse out from the matrix, leading to mass loss, as discussed in Sec. 5.2.3.

5.2.3 Modification of Molecular Weight and Mass. Degradation is characterized by sample MW and sample mass. MW
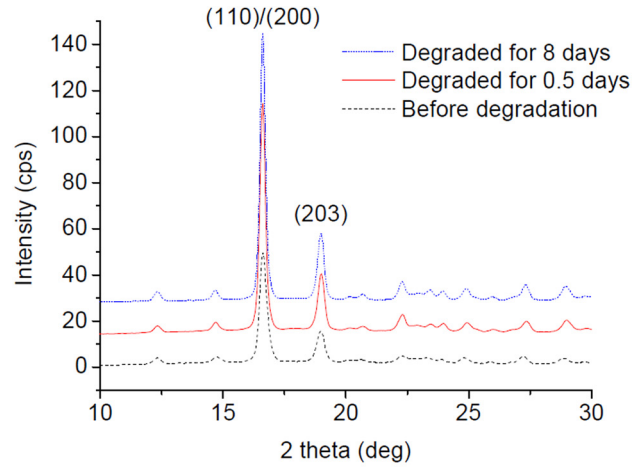
(a) Non-laser treated sample
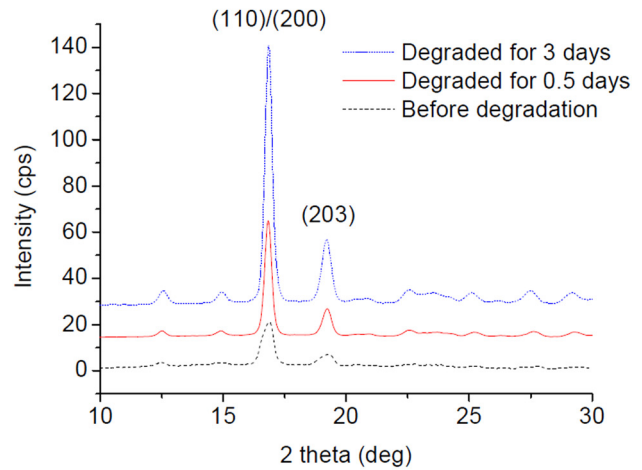
(b) Laser treated sample

Fig. 6 WAXD profiles of the (a) nonlaser-treated and (b) laser-treated (F = 3 J/cm²) samples degraded for regular periods. Intensity of crystalline peaks increases with degradation period, suggesting a higher crystallinity. Profiles are shifted in y direction for viewing clarity.
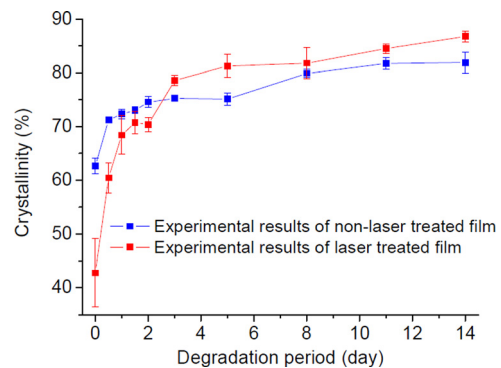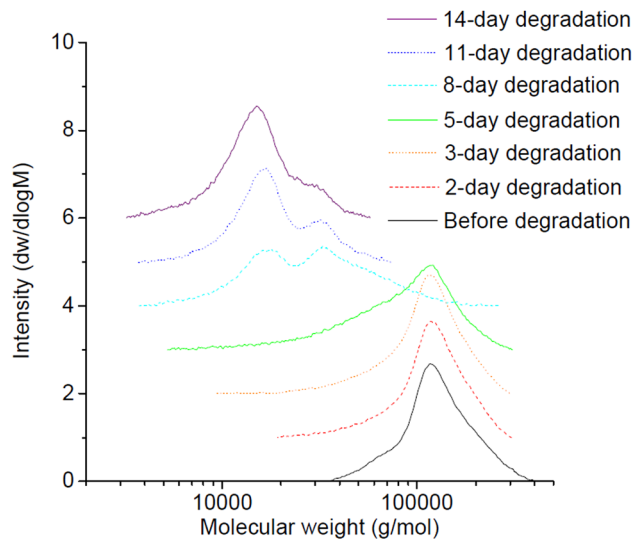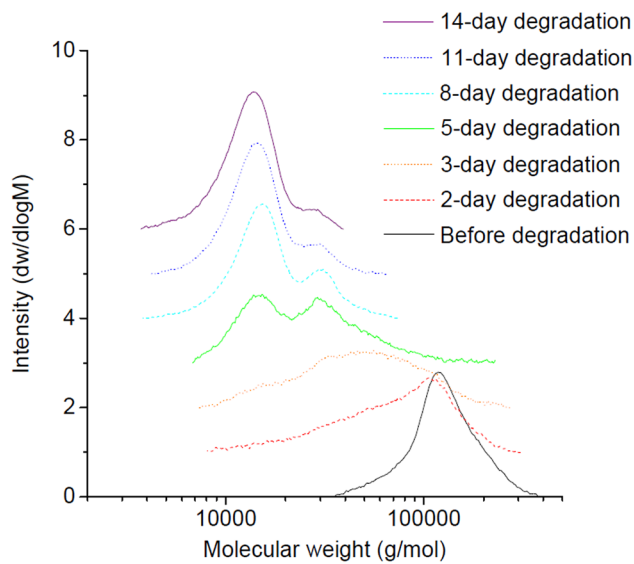

Fig. 7 Crystallinity as a function of degradation period determined from WAXD. Crystallinity increases with degradation period. A significant increase occurs on day 0.5 for both types of samples. Crystallinity also increases on day 8 and day 5 for the nonlaser-treated and laser-treated samples, respectively. The error bar represents the standard deviation of 3 data points.

Journal of Manufacturing Science and Engineering

FEBRUARY 2014, Vol. 136 / **011005-5**

distribution profiles as a function of degradation period are given in Fig. 8, which plots the mass fraction of chains (w) per increment of MW in a logarithmic scale (logM) versus MW. The number-average MW (M_n) and weight-average MW (M_w) are determined from MW distributions. The polydispersity index (PDI), defined as M_w/M_n, is calculated as a measure of distribution of MW. M_n, M_w, and PDI for the nonlaser-treated and laser-treated samples are given in Fig. 9. To better compare the MW reduction during degradation, the M_n and M_w have been normalized based on the initial M_w of the thermal-molded sample before

(a) Non-laser treated sample

(b) Laser treated sample

Fig. 9 M_w, M_n, and PDI of the (a) nonlaser-treated and (b) laser-treated samples after regular degradation periods. M_w and M_n decrease at a higher rate for the laser treated samples, as a result of fast degradation in the laser-melted layer. The nonhomogeneous degradation of the melted layer and bulk increases PDI. The error bar represents the standard deviation of 3 data points.
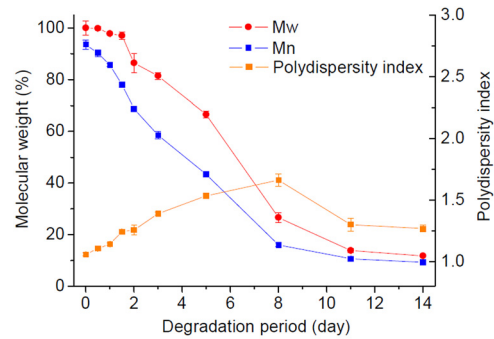

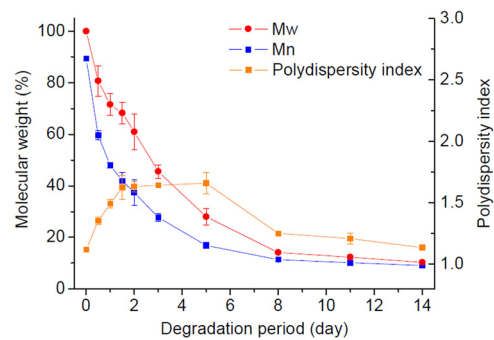(a) Non-laser treated sample

(b) Laser treated sample

Fig. 8 GPC profiles of the (a) nonlaser-treated and (b) laser-treated samples after regular degradation periods. For (a), the distribution becomes wider and shifts left as the degradation period increases to day 5, representing the random chain scission in the amorphous region. After day 8, a distinct new peak is developed due to selective chain scission of the fold surface of crystals. For (b), the MW distribution extends to the left before day 3, signifying the random chain scission of the laser melt layer. At day 5, two distinct peaks are developed due to the selective chain scission of the partially melted crystal fold surfaces. Profiles are shifted in y direction for viewing clarity.

degradation. The initial M_w of the nonlaser-treated sample is 137,000 g/mol with standard deviation of 4000 g/mol. The initial M_w of the laser-treated sample is 135,000 g/mol with standard deviation of 1000 g/mol. Sample mass as a function of degradation period is given in Fig. 10.

For nonlaser-treated samples, the GPC profile before degradation is centered at around 120,000 g/mol and the distribution is narrow, as shown in Fig. 8(a). As the degradation period increases, days 2, 3, and 5, the distribution gradually becomes wide and shifts left. A small hump is developed at around 60,000 g/mol at day 5. Sample MW decreases while PDI increases
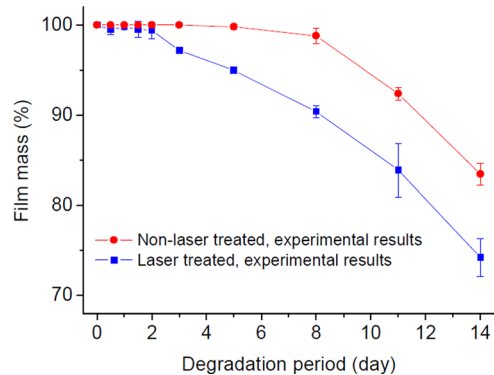

Fig. 10 Experimental results of sample mass with and without laser treatments. Mass decrease is observed after day 8 for nonlaser-treated sample and after day 3 for laser-treated sample. The error bar represents the standard deviation of 3 data points.

as a result of random chain scission, as given in Fig. 9(a). Random chain scission before day 5 occurs in the amorphous region, causing chains to degrade into segments with various MWs [18]. There is no obvious mass decrease before day 5 for nonlaser-treated sample, as given in Fig. 10, because the degraded segments are not small enough to diffuse out of the sample. The degraded segments have higher mobility and reorganize themselves from a disordered to an ordered state as a result of intermolecular hydrogen bonds and van der Waals forces during degradation, which increases the crystallinity for the first 5 days, as shown in Fig. 7.

At day 8, the GPC profile of the nonlaser-treated samples shifts left significantly, Fig. 8(a). A distinct peak, corresponding to a smaller MW of 10,300 g/mol, is observed. This shift is due to the selective scission of the crystal fold surface. Preferential scission generates chains with MW representing the integral folds the crystalline residues [18,20]. The left peak is mainly composed of the MW of crystalline residues, and the right peak mainly comes from the amorphous region experiencing random chain scission. As degradation approaches 11 and 14 days, the right peak starts to diminish due to the continuous scission of amorphous chains, and the overall distribution is mainly composed of a peak centered at 10,300 g/mol. The PDI thus decreases, as shown in Fig. 9(a).

Figure 7 shows that crystallinity increases significantly on day 8 for the nonlaser-treated sample and on day 3 for the laser-treated sample, which correspond with the time period for mass loss shown in Fig. 10. While the increase of crystallinity can be a result of the crystallization of amorphous regions, crystallinity increases on day 8 for the nonlaser-treated sample and day 3 for the laser-treated sample can be caused by the amorphous materials diffusing out of the sample, as supported by Figs. 7 and 10. The reduction of amorphous material increases the crystallinity in the sample and leads to stronger local light scattering shown in Fig. 4(d).

GPC profiles of the laser-treated sample are given in Fig. 8(b). Before degradation, the GPC profile of the laser-treated sample has a peak at 120,000 g/mol similar to the nonlaser-treated sample, which suggests that laser treatment does not modify PLLA MW. When compared with the nonlaser-treated sample, MW decreases at a high rate at the early stage for the laser-treated sample. On days 2 and 3, significant changes of GPC profiles are observed in Fig. 8(b). At day 2, the peak at 120,000 g/mol decreases, while the distribution extends to the smaller MW region. The peak diminishes at day 3, and a hump at smaller MW region is developed. During this period, a random chain scission of the laser-melted layer occurs. Nonhomogeneous degradation at the laser-melted layer and the bulk widens the MW distribution and, thus, increases the PDI, Fig. 9(b). The high degradation rate of the laser-treated sample is caused by water molecules penetrating into the less-ordered structure as a result of melting and slightly reduced MW induced by laser irradiation. Faster water penetration into the bulk is also responsible for the diminished original peak at day 3.

At day 5, the hump is split into two peaks for the laser-treated sample, as shown in Fig. 8(b). The distinct distribution of two peaks is suggestive of selective chain scission on crystal fold surfaces. Same phenomenon is observed in the nonlaser-treated sample at day 8. The earlier occurrence of this selective scission for the laser-treated sample may be due to the less-ordered structure of the partially melted crystals. For partially melted crystals, the crystal thickness is diminished, which increases the molecular loop length on the fold surface [27]. This longer loop length enlarges the free volume, the volume not occupied by polymer molecules in a polymer matrix. A larger free volume allows for easy water penetration and facilitates hydrolysis on the fold surface. Toward the late stage of the degradation, the right peak diminishes and the left peak increases, as shown in Fig. 8(b). This left peak is composed of the chains with MW representing the integral folds the crystalline residues, as well as the smallest MW distribution of chains, which can remain in the matrix. The

narrowing MW distribution at the late degradation stage decreases the PDI, as given in Fig. 9(b) after day 5.

Laser surface melting accelerates MW reduction, which in turn shortens the induction periods of mass loss. Mass loss occurs at day 3 for the laser-treated samples, compared with day 8 for the nonlaser-treated sample, Fig. 10. The decrease of sample mass is accompanied with the increase of crystallinity, Fig. 7, a phenomenon observed for both types of samples. The laser-melted layer is composed of amorphous chains, part of which degrades and diffuses out at a higher rate, while the remainder crystallizes. At day 3, the degraded products in the laser-melted layer have small enough MW such that diffusion out of the matrix occurs, which leads to the mass loss as shown in Fig. 10. After the erosion of the laser-melted layer, the sample MW and mass decrease at similar rates as the nonlaser-treated sample, as observed in Figs. 9 and 10.

It is noticed that the whole sample has been measured by the GPC, including the surface layer and the nonlaser-melted bulk. Therefore, the GPC results represent an average of the MW for the laser-melted layer with a thickness of around 100 μm on each side and the rest of the bulk. Laser irradiation has also been shown to slightly reduce the M_n and M_w. The reduction of MW, in addition to the reduction of crystallinity, also contributes to the accelerated degradation.

5.3 Simulation Results of Degradation Process. The finite element simulation has been conducted to capture laser melting and degradation processes. Laser heating allows temperature to be higher than PLLA melting temperature to melt crystals, while the highest temperature during laser heating history is around 200 °C. Simulation of laser melting has also been discussed in detail in literature [10]. Spatial degradation profiles of monomer molar concentration were calculated. A comparison of laser-treated sample and nonlaser-treated sample on day 0.5 is given in Fig. 11. For nonlaser-treated sample, the concentration is higher in the center and lower near the surface, because the monomers located near the surface easily diffuse out. For the laser-treated sample, on the other hand, the monomer concentration within the 80-μm thick layer below the surface is higher than that in the bulk. The higher monomer concentration suggests the accelerated degradation in the laser-melted layer, and the simulated thickness is similar to the 100-μm thickness of laser penetration depth experimentally determined. In the later stage of degradation, the monomer concentration in the nonmelted bulk starts to increase, as a result of degradation in the bulk. The effect of laser surface melting and the difference between the laser-treated and nonlaser-treated samples thus diminish.

Simulation results of MW change as a function of degradation period are given in Fig. 12. Numerical results of the laser-treated sample experience a larger MW decrease, in agreement with experiments shown in Fig. 9. Experimentally, the MW of the nonlaser-treated sample does not decrease as significantly as predicted in simulation before day 1. This difference is because it takes time for water molecules to diffuse into the bulk in experiments. Water diffusion time is not considered in simulation, which causes the overestimation of the MW decrease.

The simulated mass changes with degradation, Fig. 13, capture the phenomenon that appreciable mass decrease occurs after an induction period experimentally obtained, Fig. 10. During the induction period in which mass loss does not occur, the original amorphous polymer chains degrade into fragments not small enough for diffusion out of the sample. Fragments experience further degradation into monomers, which can diffuse and lead to mass loss. Experimentally, the mass change is more significant when compared with simulation. This is because the erosion of crystalline material also occurs on the surface during degradation [28], which is not considered in simulation, leading to a conservative prediction.

The molar concentration of species considered in the simulation is plotted with the degradation period, given in Fig. 14(a).
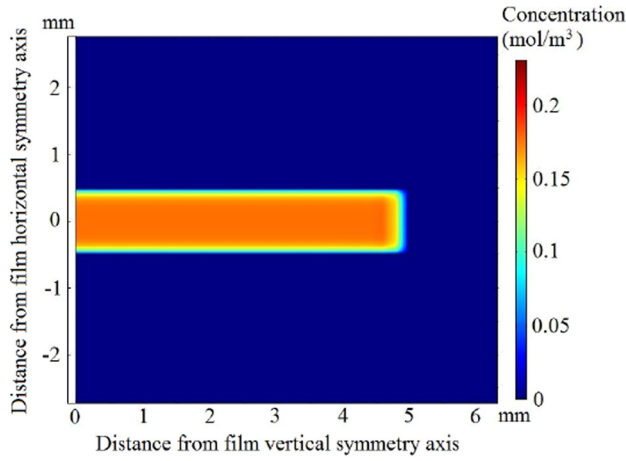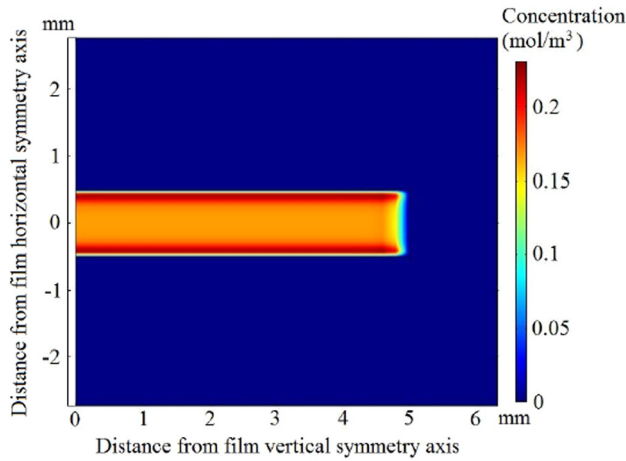
Fig. 11 Simulated spatial distribution of monomer concentration in the (*a*) nonlaser-treated sample and (*b*) laser-treated sample degraded for 0.5 days
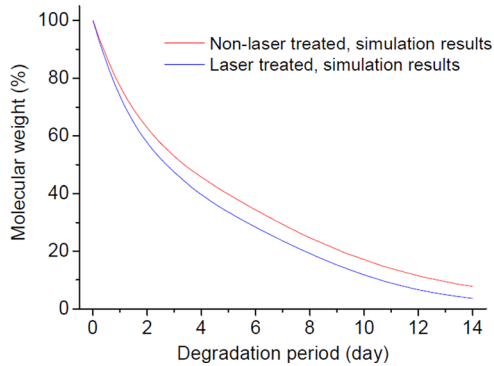

Fig. 12 Simulated MW of the nonlaser-treated and laser-treated samples

Amorphous chains start to degrade in the early stage of the degradation period, generating the species in stage 1. Stage 1 is sequentially degraded into stages 2 and 3. Chains in stage 3, upon further hydrolysis, are decomposed into monomers, which diffuse out of the sample. Only a small amount of monomers remain on the sample surface. Degradation also enhances chain mobility, which leads to crystallization. The simulated concentration of crystalline chains increases as observed in experiments. Multiple stages of
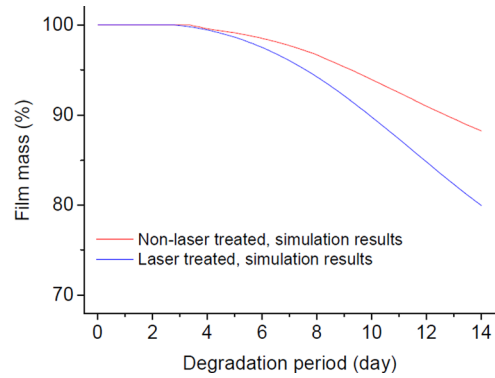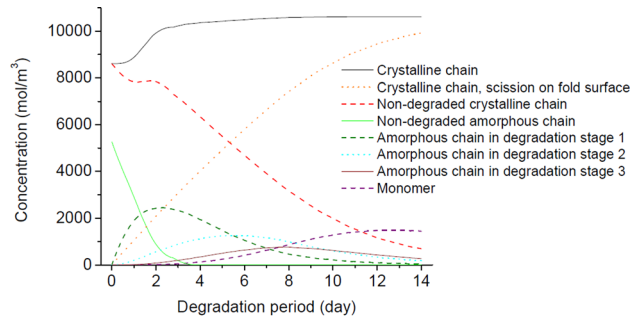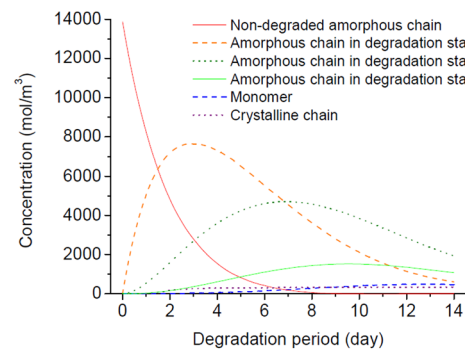

Fig. 13 Simulated mass change of the nonlaser-treated and laser-treated samples

(a) In the center of the non-laser treated sample

(b) In the laser melted layer of the laser treated sample

Fig. 14 Molar concentration of the simulated species as a function of degradation period

hydrolytic degradation have been assumed in simulation based on cellulose hydrolysis [17]. While the simulation results, under the current assumption, capture the experimental results, hydrolysis of PLLA may behavior differently and, thus, requires further investigation.

Simulated crystallinity increases via two stages, as agreed with the experiments. The first stage is predicted by the Avrami crystallization theory [25]. Experimentally, crystallinity increases to a significant extent before day 0.5, not captured in the simulation. The discrepancy results from the fact that according to the Avrami theory, crystallization begins with an induction period due to the formation of nuclei. Preexisting nuclei in the experiment samples favor crystal growth without experiencing the induction period. The second stage of crystallinity increase is due to the loss of amorphous material, which increases crystallinity as experimentally observed and numerically simulated. Hydrolysis of crystals occurs on the fold surfaces. Concentration of the nondegraded crystalline chains decreases, which leads to the increased concentration of the hydrolyzed crystals and the reduced MW.

Simulation results of the species concentration in the laser-melted layer are shown in Fig. 14(*b*). Laser irradiation melts the crystal structure, generating an amorphous layer near the surface. Amorphous chains are degraded to stages 1, 2, and 3 and monomers in sequence. Because the species are near the surface, the major part of monomers readily diffuses out of the sample and thus the concentration is lower as compared with that in the sample bulk. Although most amorphous chains degrade, crystallization takes place in the laser-melted layer, mainly at the early stage.

Based on the experimental and simulation results, laser melting accelerates PLLA degradation and the occurrence of its mass loss. The highest temperature achieved during laser heating in this study was controlled to be about 200 °C, which is within the range of proposed thermal extrusion process [29]. To apply the laser melting process in drug delivery application, the decomposition temperature of drug molecules needs to be lower than the polymer melting temperature. Biodegradable polymer with lower melting temperature, such as polycaprolactone with melting temperature of around 60 °C can be used for less thermally stable drugs.

6 Conclusions

The effect of laser irradiation on PLLA biodegradation has been studied experimentally and numerically. Excimer laser irradiation has been shown to melt the PLLA surface. The melted layer showed lower crystallinity and no observable chemical changes according to WAXD and XPS measurements. Optical micrographs taken during degradation testing show that degradation initiates on the sample surface, and the melted layer allows for the accelerated initial degradation as is also captured through numerical simulations. The laser-treated samples experience a faster initial MW reduction, which leads to a shorter induction period of mass loss as observed from GPC. Heterogeneous degradation of PLLA samples caused by inhomogeneous crystallinity is observed in both the laser-treated and nonlaser-treated samples from bimodal distribution of MW from GPC measurements. The laser-treated samples exhibited higher crystallinity after degradation as a result of preferred degradation and higher chain mobility in the amorphous phase, as confirmed from the WAXD measurements. Changes in MW, sample mass, and species evolution during degradation are captured in simulation results of both the laser-treated and nonlaser-treated samples. Laser modification to the crystallinity of PLLA has been shown to reduce the degradation induction period, a desired property in drug delivery applications.

References

[1] Amass, W., Amass, A., and Tighe, B., 2008, "A Review of Biodegradable Polymers: Uses, Current Developments in the Synthesis and Characterization of Biodegradable Polyesters, Blends of Biodegradable Polymers and Recent Advances in Biodegradation Studies." Polym. Int., **47**, pp. 89–144.

[2] Lao, L. L., Venkatraman, S. S., and Peppas, N. A., 2009, "A Novel Model and Experimental Analysis of Hydrophilic and Hydrophobic Agent Release From Biodegradable Polymers," J. Biomed. Mater. Res. A, **90**, 1054–1065.

[3] Chu, C. C., 1981, "Hydrolytic Degradation of Polyglycolic Acid: Tensile Strength and Crystallinity Study," J. Appl. Polym. Sci., **26**, pp. 1727–1734.

[4] Tsuji, H., and Ikada, Y., 1998, "Properties and Morphology of Poly(L-Lactide). II. Hydrolysis in Alkaline Solution," J. Polym. Sci. A: Polym. Chem., **36**, pp. 59–66.

[5] Siparsky, G. L., Voorhees, K. J., and Miao, F., 1998, "Hydrolysis of Polylactic Acid (PLA) and Polycaprolactone (PCL) in Aqueous Acetonitrile Solutions: Autocatalysis," J. Environ. Polym. Degrad., **6**, pp. 31–41.

[6] Zong, X. H., Wang, Z. G., Hsiao, B. S., Chu, B., Zhou, J. J., and Jamiolkowski, D. D., 1999, "Structure and Morphology Changes in Absorbable Poly(Glycolide) and Poly(Glycolide-co-Lactide) During in Vitro Degradation," Macromolecules, **32**, pp. 8107–8114.

[7] Renouf-Glausera, A. C., Roseb, J., Farrarb, D. F., and Cameron, R. E., 2005, "The Effect of Crystallinity on the Deformation Mechanism and Bulk Mechanical Properties of PLLA," Biomaterials, **26**, pp. 5771–5782.

[8] Bhatla, A., and Yao, Y. L., 2009, "Effect of Laser Surface Modification on the Crystallinity of Poly(L-Lactic Acid)," ASME J. Manuf. Sci. Eng., **131**, 051004.

[9] Dunn, D. S., and Ouderkirk, A. J., 1990, "Chemical and Physical Properties of Laser-Modified Polymers," Macromolecules, **23**, pp. 770–774.

[10] Hsu, S.-T., Tan, H., and Yao, Y. L., 2012, "Effect of Excimer Laser Irradiation on Crystallinity and Chemical Bonding of Biodegradable Polymer," Polym. Degrad. Stab., **97**, pp. 88–97.

[11] Weir, N. A., Buchanan, F. J., Orr, J. F., Farrar, D. F., and Dickson, G. R., 2004, "Degradation of Poly-L-Lactide. Part 2: Increased Temperature Accelerated Degradation," Proc. Inst. Mech. Eng., Part. H: J. Eng. Med., **218**, pp. 321–330.

[12] Yamamoto, T., 2010, "Molecular Dynamics of Reversible and Irreversible Melting in Chain-Folded Crystals of Short Polyethylene-Like Polymer," Macromolecules, **43**, pp. 9384–9393.

[13] Pitt, C. G., and Gu, Z., 1987, "Modification of the Rates of Chain Cleavage of Poly(ε-Caprolactone) and Related Polyesters in the Solid State," J. Controlled Release, **4**, pp. 283–292.

[14] Li, S. M., Garreau, H., and Vert, M., 1990, "Structure-Property Relationships in the Case of the Degradation of Massive Poly(α-Hydroxy Acids) in Aqueous Media: Part 2 Degradation of Lactide-Glycolide Copolymers: PLA37.5GA25 and PLA75GA25," J. Mater. Sci.: Mater. Med., **1**, pp. 131–139.

[15] Lyu, S., Schley, J., Loy, B., Lind, D., Hobot, C., Sparer, R., and Untereker, D., 2007, "Kinetics and Time-Temperature Equivalence of Polymer Degradation," Biomacromolecules, **8**, pp. 2301–2310.

[16] Wang, Y., Pan, J., Han, X., Sinka, C., and Ding, L., 2008, "A Phenomenological Model for the Degradation of Biodegradable Polymers," Biomaterials, **29**, pp. 3393–3401.

[17] Stephens, C. H., Whitmore, P. M., Morris, H. R., and Bier, M. E., 2008, "Hydrolysis of the Amorphous Cellulose in Cotton-Based Paper," Biomacromolecules, **9**, pp. 1093–1099.

[18] Tsuji, H., and Tsuruno, T., 2010, "Accelerated Hydrolytic Degradation of Poly(L-Lactide)/Poly(D-Lactide) Stereocomplex up to Late Stage," Polym. Degrad. Stab., **95**, pp. 477–484.

[19] Tsuji, H., and Ikarashi, K., 2004, "In Vitro Hydrolysis of Poly(L-Lactide) Crystalline Residues as Extended-Chain Crystallites: II. Effects of Hydrolysis Temperature," Biomacromolecules, **5**, pp. 1021–1028.

[20] Fischer, E. W., Sterzel, H. J., and Wegner, G., 1973, "Investigation of the Structure of Solution Grown Crystals of Lactide Copolymers by Means of Chemical Reactions," Kolloid Z. Z. Polym., **251**, pp. 980–990.

[21] Toda, A., Tomita, C., Hikosaka, M., and Saruyama, Y., 1998, "Melting of Polymer Crystals Observed by Temperature Modulated D.S.C. and Its Kinetic Modeling," Polymer, **39**, pp. 5093–5104.

[22] Li, S., and McCarthy, S., 1999, "Influence of Crystallinity and Stereochemistry on the Enzymatic Degradation of Poly(lactide)s," Macromolecules, **32**, pp. 4454–4456.

[23] Avrami, M., 1941, "Granulation, Phase Change, and Microstructure: Kinetics of Phase Change. III," J. Chem. Phys., **9**, pp. 177–184.

[24] Alexander, L. E., 1969, *X-Ray Diffraction Methods in Polymer Science*, Wiley, New York, Chap. 1.

[25] Avrami, M., 1939, "Kinetics of Phase Change. I: General Theory," J. Chem. Phys., **7**, pp. 1103–1112.

[26] Menczel, J., and Wunderlich, B., 1981, "Heat Capacity Hysteresis of Semicrystalline Macromolecular Glasses," J. Polym. Sci.: Polym. Lett. Ed., **19**, pp. 261–264.

[27] Belyayev, O. F., 1988, "Mechanism of Melting of Oriented Polymers," Polym. Sci. U.S.S.R., **30**, pp. 2545–2552.

[28] Lam, C. X. F., Savalani, M. M., Teoh, S. H., and Hutmacher, D. W., 2008, "Dynamics of in vitro Polymer Degradation of Polycaprolactone-Based Scaffolds: Accelerated Versus Simulated Physiological Conditions," Biomed. Mater., **3**, 034108.

[29] Breitenbach, J., and Lewis, J., 2003, *Modified-Release Drug Delivery Technology*, M. J. Rathbone, J. Hadgraft, and M. S. Roberts, eds., Marcel Dekker, New York, Chap. 11.